Desalination and Water Treatment
www.deswater.com

doi: 10.5004/dwt.2021.26635

212 (2021) 333–346
February

Mechanism of oxidative decomposition of direct red 89 by Bi_2O_3/TiO_2 composite under visible light irradiation: effect of co-existing cations and anions and artificial neural network modeling of key factor

Asiyeh Bazmeh[a,b], Ali Fatehizadeh[a,c], Bijan Bina[a,c,*], Bahareh Shoshtari-Yeganeh[c]

[a]*Department of Environmental Health Engineering, School of Health, Isfahan University of Medical Sciences, Isfahan, Iran, Tel. +98 31 3792 3275; Fax: +98 31 3669 5849; emails: bbina123@yahoo.com (B. Bina), as.bazmeh@gmail.com (A. Bazmeh), a.fatehizadeh@hlth.mui.ac.ir (A. Fatehizadeh)*
[b]*Student Research Committee, School of Health, Isfahan University of Medical Sciences, Isfahan, Iran*
[c]*Environment Research Center, Research Institute for Primordial Prevention of Non-Communicable Disease, Isfahan University of Medical Sciences, Isfahan, Iran, email: Baharshoshtary@gmail.com*

Received 3 February 2020; Accepted 2 October 2020

ABSTRACT

In the present study, the Bi_2O_3/TiO_2 composite was successfully synthesized by the solvothermal method and used for photocatalytic degradation of direct red 89 (DR89) from aqueous solution under visible light and UV-C irradiation. The effects of influencing parameters including solution pH, Bi_2O_3/TiO_2 dose, initial DR89 concentration, reaction time, co-existing cations and anions, and persulfate (PS) dose were examined. Finally, the artificial neural network (ANN) model was developed for the prediction of the photocatalytic removal of DR89. The results showed that with increasing solution pH from 3 to 4, the DR89 degradation promptly enhanced from 33.8% to 54.4% and after that, vigorously declined to 2.5% at a pH of 8. In addition, the increase of Bi_2O_3/TiO_2 dose from 100 to 800 mg/L led to the DR89 degradation efficiency increase from 60.7% to 94.8%. It was found that for achieving a high DR89 degradation efficiency under visible light irradiation at 20 mg/L of DR89, the solution pH and reaction time should be 4 and 45 min, respectively. When PS was added in the photocatalysis process, the highest removal efficiency of DR89 was observed at PS dose of 2.5 mg/L under UV-C irradiation. The presence of co-existing anions in the medium inhibited the DR89 removal efficiency following a trend that $PO_4^{3-} > Cl^- > SO_4^{2-}$ and for co-existing cations was in the order of $Na^+ > Ca^{2+} > Mg^{2+}$. The decomposition of the DR89 obeyed the first-order reactions and the rate constant was 0.012 mg/L min. The correlation coefficient for ANN was calculated 0.993, confirming that the predicted data from the designed ANN model were in good agreement with the experimental data.

Keywords: ANN model; Bi_2O_3/TiO_2 composite; Co-existing cations and anions; Direct red 89

1. Introduction

Nowadays, dyes are considered as one of the biggest environmental polluters and are widely used in many industries like textiles, food, leather, plastics, paper, pharmaceutical, and cosmetics [1,2]. The textile industry is the greatest consumer of dyes and as a result, high volumes of wastewater were produced in the different dyeing steps [3]. The main characteristics of dye compounds are carcinogenic behavior and low biodegradability [4]. Hence, its efficient treatment is mandatory before discharging textile wastewater into the environment [1].

* Corresponding author.

The photocatalysis process based on the TiO_2 nanoparticles is considered an efficient treatment method for textile effluents due to eco-friendly and cost-effective in nature. The main characteristics of TiO_2 nanoparticles including low toxicity, low cost, and stability against photolytic lead to its widely used for the degradation of organic pollutants [5,6]. However, the dominants drawbacks of TiO_2 application are first, exciting the large bandgap (about 3.2 eV) with UV light, and second, increasing the recombination probability of the photo-generated electrons due to the simultaneous conducting of photooxidation and photoreduction on the reaction site of TiO_2 surface. In order to improve the photocatalytic characteristics of the TiO_2 catalyst and overcome the mentioned problems, the researchers proposed some solutions including TiO_2 linking with magnetic metals, semiconductors doping, and stabling on carbon-based nanomaterials. Furthermore, the coupling of TiO_2 by semiconductors with narrow bandgap can be used for modifying TiO_2 activity in visible light [7]. Among semiconductors, Bi_2O_3 has been proposed as the most important photocatalysts due to a narrow bandgap and visible light absorbability [8]. Comparing to Bi_2O_3, the TiO_2 has a low energy level of the conduction band and leads to the transfer of the photogenerated electrons from Bi_2O_3 to TiO_2 and consequently, the TiO_2 performance under visible light irradiation improved [9].

In the previous study, many light sources such as xenon and fluorescent lamps have been used and depicted operational difficulties including high-temperature production, UV light generation, and high costs related to the reflector for photocatalyst nanoparticle activation. In order to overcome the above-mentioned concerns, some researchers have proposed the light-emitting diodes (LED) lamp as a light source [10,11] and demonstrated that the LED lamps have a longer lifespan, lower consumption of power, smaller size, superior physical strength, and faster switching comparing to traditional light sources [12].

The artificial neural network (ANN) model as a powerful statistical tool is proposed based on the human brain and used for establishing the complex nonlinear relationships between independent and dependent influencing factors. The ANN is optimized with training the model by introducing some part of experimental data to find the nonlinear correlations between the input and output data sets [13]. The dominant advantages of the ANN are simplicity in operation, high ability to learn the patterns with minor adaptations, effective estimate of complex systems even without the variables relationship recognition, and independence from any regular experimental design [14–16].

In the present study, the researchers focused on the synthesis of Bi_2O_3/TiO_2 catalysts by the solvothermal method and used the synthesized composites for direct red 89 (DR89) degradation efficiency from aqueous solutions under UV and visible light irradiations. The effect of some parameters such as initial DR89 concentration, solution pH, reaction time, Bi_2O_3/TiO_2 dose, and co-existing inorganic ions was studied. In addition, the combination of Bi_2O_3/TiO_2 photocatalysis and persulfate for DR89 removal was examined. An important objective was to obtain an ANN model which could make a reliable prediction of DR89 degradation efficiency of the Bi_2O_3/TiO_2 photocatalysis process.

2. Materials and methods

2.1. Chemicals

In the present work, tetrabutyl titanate ($Ti(OC_4H_9)_4$), bismuth nitrate ($Bi(NO_3)_3 + 5H_2O$), acetic acid (HAc), and polysorbate 80 (T80) for catalysis synthesis were purchased from Sigma-Aldrich (St. Louis, Missouri, USA) without further treatment. Sodium chloride (NaCl), calcium chloride ($CaCl_2 + 2H_2O$), potassium dihydrogen phosphate (KH_2PO_4), manganese sulfate ($MnSO_4 + 4H_2O$), potassium nitrate (KNO_3), magnesium sulfate ($MgSO_4$), ammonium chloride (NH_4Cl), NaOH, HCl, and sodium persulfate ($Na_2S_2O_8$) were collected from Merck Co. (Darmstadt, Germany). The DR89 (a double azo class, molecular formula: $C_{44}H_{32}N_{10}Na_4O_{16}S_4$, molecular weight: 1,177 g/mol, CAS registry number: 12217-67-3, and λ_{max}: 494 nm) was obtained from Baharjin Textile Factory, (Iran).

2.2. Bi_2O_3/TiO_2 catalyst synthesis

The schematic illustration of Bi_2O_3/TiO_2 catalyst fabrication is shown in Fig. 1. The Bi_2O_3/TiO_2 was chemically prepared using $Bi(NO_3)_3 + 5H_2O$ and $Ti(OC_4H_9)_4$ [17].

The synthesized Bi_2O_3/TiO_2 catalyst was subjected to transmission electron microscopy (TEM), energy-dispersive X-ray spectroscopy (EDX), Brunauer–Emmett–Teller (BET) test.

2.3. Photocatalysis experiments

The removal efficiency of the synthesized Bi_2O_3/TiO_2 catalyst was evaluated by monitoring the photodegradation of DR89 in an aqueous solution using LED (125 W) and UV lamp (150 W, UV_{max}, 254 nm). The photodegradation experiments were carried out in a glass vessel (1,000 mL

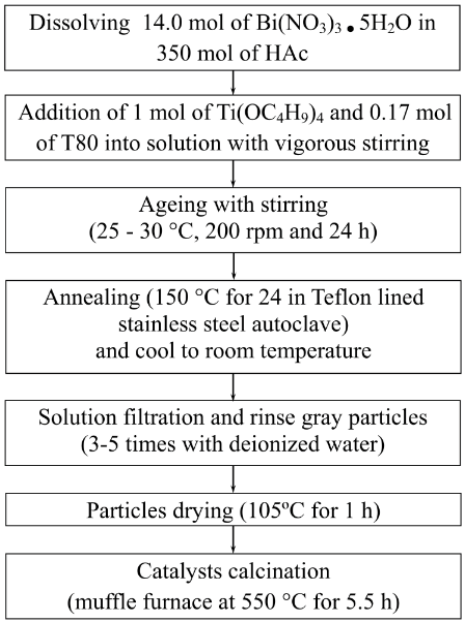

Fig. 1. Schematic representation of Bi_2O_3/TiO_2 catalyst fabrication.

with 10 cm inside diameter). The light source distance from the top solution surface was fixed to 12 cm. In order to provide perfect mixing, a magnetic stirrer was used (200 rpm) during all experiments. Several sets of photodegradation experiments were conducted to determine the effects of primary parameters on DR89 removal including solution pH, reaction time, initial DR89 concentration, Bi_2O_3/TiO_2 dose, light source type, a dose of persulfate (PS), and co-existing cations and anions. The employed experimental conditions for DR89 removal by Bi_2O_3/TiO_2 photocatalysis are summarized in Table 1.

Before conducting the experiments, the solution was put in a dark chamber for 30 min to achieving adsorption-desorption equilibrium between the Bi_2O_3/TiO_2 catalyst and the DR89 molecule. The residual DR89 concentration in samples was quantified using a visible spectrophotometer (Milton Roy Company 2OD) at the wavelength (λ_{max}) of 494 nm.

2.4. Protocol of ANN modeling

The ANN modeling and calculations were carried out using Matlab 14 mathematical software with neural fitting toolbox (*nftool*). In the present study, a three-layer feed-forward network with a sigmoid hidden neuron transfer function (*trainscg*) and linear output neurons (*fitnet*), with Levenberg–Marquardt back-propagation algorithm (*trainlm*) was constructed.

3. Results and discussion

3.1. Characterization of Bi_2O_3/TiO_2 catalyst

In order to observe the surface morphology of Bi_2O_3/TiO_2 composite, TEM micrographs were taken and are illustrated in Fig. 2.

As seen in Fig. 2, the Bi_2O_3/TiO_2 catalyst particles have a hexagonal shape with typical lengths in the range of 22–150 nm. Karunakaran et al. [18] reported that Bi_2O_3/TiO_2 particles are spherical in shape with a size between 72 and 110 nm. In addition, Sood et al. [19] synthesized Bi_2O_3/TiO_2 using the hydrothermal method and concluded that the nanoparticles formed aggregates or clusters with sized particles ranging from 8 to 15 nm.

In order to calculate the BET specific surface area, pore size, and pore volume of Bi_2O_3/TiO_2 composite particles, the

Table 1
Experimental conditions employed in DR89 removal by Bi_2O_3/TiO_2 photocatalysis process

Studied parameter	Experimental conditions							
	Solution pH	Reaction time (min)	DR89 conc. (mg/L)	Bi_2O_3/TiO_2 dose (mg/L)	Light source	Persulfate dose (mg/L)	Cation type	Anion type
Solution pH	3	30	20	100	LED	–	–	–
Reaction time	4	5–90	20	100	LED	–	–	–
Bi_2O_3/TiO_2 dose	4	45	20	100–800	LED	–	–	–
DR89 concentration	4	45	10–60	800	LED	–	–	–
Light source	4	45	10–30	800	LED, UV	–	–	–
Co-existing cations	4	45	20	800	LED, UV	–	Na^+, K^+, Ca^{2+}, Mg^{2+}	–
Co-existing anions	4	45	20	800	LED, UV	–	–	Cl^-, SO_4^{2-}, PO_4^{3-}
PS dose	4	45	20	100	LED, UV	2.5–12.5	–	–

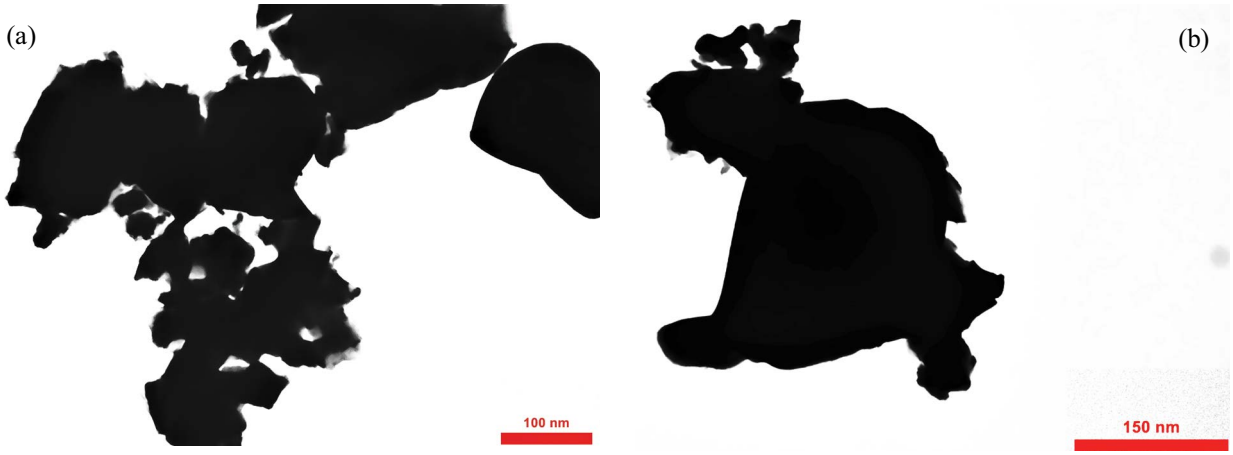

Fig. 2. TEM image of catalyst Bi_2O_3/TiO_2 catalyst (a) 100 nm and (b) 150 mn magnification.

N_2 gas adsorption analyzer was used. The pore size distribution curves and N_2 adsorption–desorption isotherms Bi_2O_3/TiO_2 composite are shown in Fig. 3.

The BET examination indicated that the BET surface area (S_{BET}), total pore volume (V_{total}), and mean pore diameter were 1.56 m^2/g, 0.011 cm^3/g, and 29.26 nm, respectively. The S_{BET} of commercial Bi_2O_3 (0.4 m^2/g) was lower than Bi_2O_3 modified by TiO_2 [20]. A high S_{BET} of catalyst provides more active sites, which are a clear reason for enhancing the photocatalytic performance [21]. In addition, the S_{BET} of Bi_2O_3/TiO_2 was lower than pure TiO_2 (82 m^2/g) [22]. According to Ayekoe et al. [22] study, when the Bi/Ti ratio increased, the S_{BET} had reduced, probably due to the low surface area of bismuth oxide. Sood et al. [19] observed that the S_{BET}, V_{total}, and mean pore diameter of synthesized Bi_2O_3/TiO_2 composite were 156.8 m^2/g, 0.394 cm^3/g, and 13.78 nm, respectively. Furthermore, Ayekoe et al. [22] reported that V_{total}, S_{BET}, and mean pore diameters were 0.153 cm^3/g, 87 m^2/g, and 3.5–7.5 nm, respectively. The EDX pattern of the Bi_2O_3/TiO_2 catalyst is depicted in Fig. 4.

As seen in Fig. 4, the peaks of Bi, Ti, and O could be clearly seen which indicated the chemical composition of Bi_2O_3/TiO_2 catalyst includes oxygen (11.62%), titanium (0.19%), and bismuth (87.99%). According to Sood et al. [19], the Bi_2O_3/TiO_2 catalyst included 19.76%, 33.19%, and 47.04 % of Bi, Ti, and O elements, respectively.

3.2. Photocatalysis process performance

In the present study, the efficiency of Bi_2O_3/TiO_2 photocatalytic by using LED and UV lamp as a light source in the degradation of DR89 dye from aqueous solution was systematically investigated (Table 1).

3.2.1. Effect of solution pH

The previous studies have reported that solution pH significantly affects the photocatalytic process by changing the surface charge properties of the semiconductor [23,24]. In order to examine the effect of solution pH on the degradation efficiency of DR89 by Bi_2O_3/TiO_2 photocatalysis, the experiments were carried out by changing solution pH from 3 to 8 under LED light irradiation and the obtained results are illustrated in Fig. 5.

As seen in Fig. 5, the degradation efficiency of DR89 increased at acidic pH and decreased at alkaline pH. With increasing solution pH from 3 to 4, the DR89 removal efficiency was enhanced and then promptly depleted. The highest and lowest DR89 removal efficiency by Bi_2O_3/TiO_2 photocatalysis was obtained at a solution pH of 4 and 8 and equal to 54.4% and 2.5% removal efficiency, respectively. Thus, the DR89 removal efficiency by Bi_2O_3/TiO_2 is more favorable under acidic conditions. This behavior is related to the pH of PZC (pH_{PZC}) of Bi_2O_3/TiO_2 composites. The pH_{PZC} of Bi_2O_3/TiO_2 composites was 6.8 and the solution pH lower than pH_{PZC} resulted in the positive charge of Bi_2O_3/TiO_2 composites [25]. The existence of positive charges under acidic pH on the surface of Bi_2O_3/TiO_2 composites and the negative charges of DR89 dye molecules resulted in the vigorous electrostatic interactions between them and led to higher DR89 degradation [26].

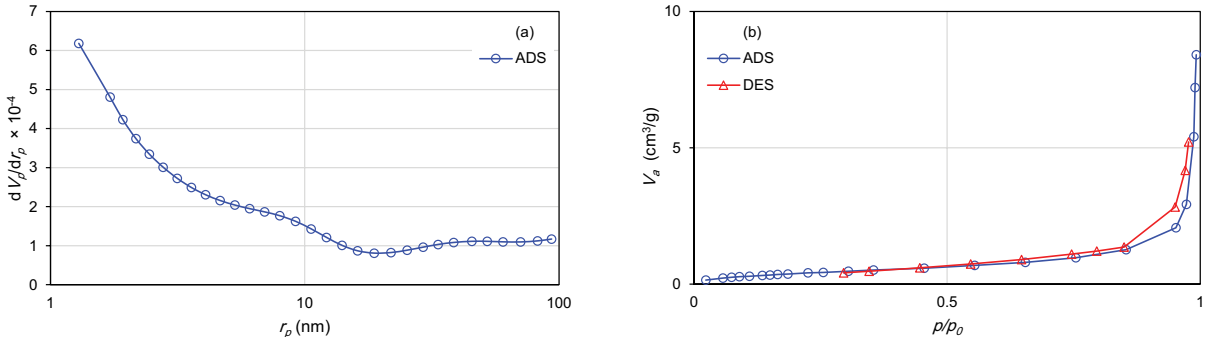

Fig. 3. (a) Pore size distribution curves and (b) N_2 adsorption–desorption isotherms.

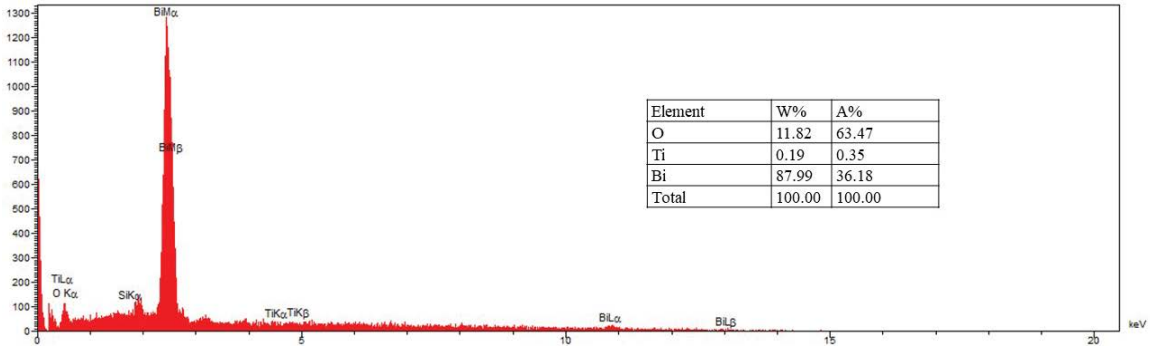

Element	W%	A%
O	11.82	63.47
Ti	0.19	0.35
Bi	87.99	36.18
Total	100.00	100.00

Fig. 4. Energy-dispersive X-ray spectroscopy pattern of Bi_2O_3/TiO_2 catalyst.

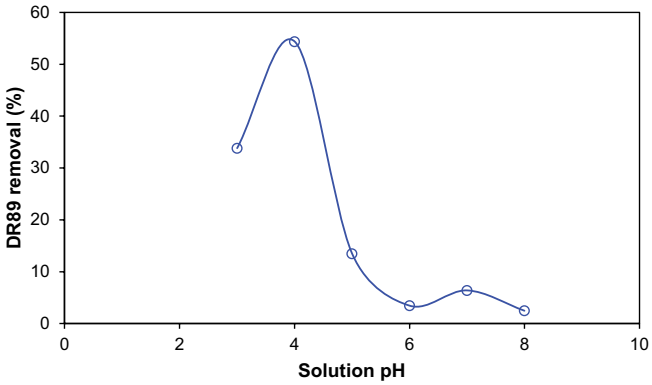

Fig. 5. Variation of DR89 removal by Bi_2O_3/TiO_2 photocatalysis (DR89 concentration: 20 mg/L; Bi_2O_3/TiO_2 dose: 100 mg/L; reaction time: 30 min; LED as light source).

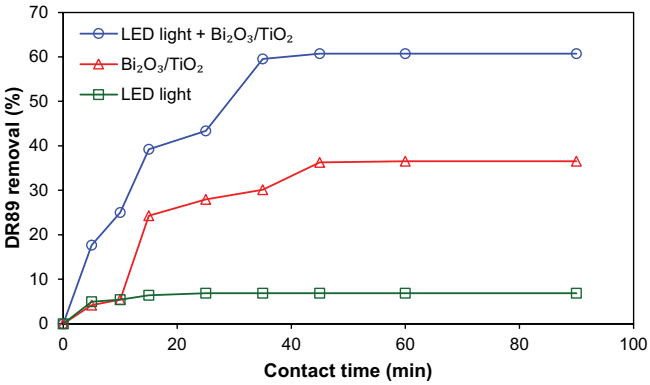

Fig. 6. DR89 removal efficiency as a function reaction time by Bi_2O_3/TiO_2 photocatalysis and Bi_2O_3/TiO_2 and LED light alone (DR89 concentration: 20 mg/L; Bi_2O_3/TiO_2 dose: 100 mg/L; solution pH: 4).

Conversely, the application of solution with pH values above pH_{PZC} and the surface of Bi_2O_3/TiO_2 composites was charged positively [27]. In this condition, the electrostatic repulsion between Bi_2O_3/TiO_2 composites surface and DR89 dye was predominant, indicating the unfavorable condition for DR89 removals by Bi_2O_3/TiO_2 photocatalysis under LED light irradiation from aqueous solution [28]. Sajjad et al. [29] reported that the highest methyl orange degradation efficiency was obtained for 25 mg/L of initial concentration at a pH of 4.

3.2.2. *Effect of reaction time on Bi_2O_3/TiO_2 photocatalysis efficiency*

In order to determine the optimum reaction time for DR89 removal by the Bi_2O_3/TiO_2 photocatalysis, a series of experiments were conducted at various reaction times under optimum solution pH. In addition, the DR89 removal efficiency was examined by Bi_2O_3/TiO_2 adsorption and LED radiation alone. Fig. 6 depicts the DR89 removal efficiency by LED light, Bi_2O_3/TiO_2 adsorption, and Bi_2O_3/TiO_2 photocatalysis.

As illustrated in Fig. 6, in each process, the DR89 removal efficiency was enhanced with reaction time increment. In addition, the Bi_2O_3/TiO_2 photocatalysis was exhibited higher DR89 removal efficiency in comparison with LED radiation and Bi_2O_3/TiO_2 adsorption. In case of Bi_2O_3/TiO_2 photocatalysis, the DR89 removal efficiency was intensively enhanced from 17.7% to 60.77% with increasing reaction time from 5 to 45 min and no significant removal efficiency enhancement was observed with increasing reaction time up to 90 min. During the trials involving Bi_2O_3/TiO_2 photocatalysis, a reaction time of 45 min was selected as optimum reaction time.

Many active sites are available on the surface of the catalyst which can a reason for the high degradation rate of the DR89 dye [30]. In case of Bi_2O_3/TiO_2 photocataysis process under visible light irradiation, the DR89 removal was constant with increasing reaction times from 45 to 90 min (60.77%) since the active sites became saturated gradually [31]. The obtained data are in line with Pirinejad et al. [32], who reported that the degradation efficiency of acid black 1 improved from 19.8% to 71% with increasing reaction time from 10 to 60 min but the efficiency slightly increased and with increasing reaction time to 120 min.

3.2.3. *Kinetic study*

The kinetic study of Bi_2O_3/TiO_2 photocatalysis was processed with the zero-order, first-order, and second-order kinetic model to understand the constant rate of DR89 removal by Bi_2O_3/TiO_2 photocatalysis. The equation of kinetic models Eqs. (1)–(3) being used in the present study are summarized in Table 2.

Table 2
Integration and differential methods used to determine reaction rate coefficients

Rate expression	Integration method	Integrated form	Equations
Zero-order	$r_c = \frac{dC}{dt} = k_0$	$C - C_0 = -k_0 t$	(1)
First-order	$r_c = \frac{dC}{dt} = k_1 C$	$\ln \frac{C}{C_0} = k_1 t$	(2)
Second-order	$r_c = \frac{dC}{dt} = k_2 C^2$	$\frac{1}{C} - \frac{1}{C_0} = k_2 t$	(3)

Table 3
Rate constants of kinetics models for DR89 removal by LED radiation, Bi_2O_3/TiO_2 adsorption, and Bi_2O_3/TiO_2 photocatalysis

Kinetic type	Parameters	Value		
		LED light	Bi_2O_3/TiO_2 adsorption	Bi_2O_3/TiO_2 photocatalysis
Zero-order	k_0	0.009 ± 0.005	0.085 ± 0.02	0.125 ± 0.03
	Reduced Chi-Square	0.15	3.22	7.42
	R^2_{adj}	0.25	0.64	0.67
First-order	k_1	0.0004 ± 0.0001	0.006 ± 0.01	0.012 ± 0.0001
	Reduced Chi-Square	0.15	0.022	0.205
	R^2_{adj}	0.25	0.99	0.98
Second-order	k_2	0.00003 ± 0.0001	0.0003 ± 0.0001	0.0011 ± 0.0001
	Reduced Chi-Square	0.15	0.022	0.69
	R^2_{adj}	0.24	0.98	0.93

where C_0 and C indicate the influent and effluent concentration of DR89, respectively, k_0, k_1, and k_2 represent the rate constant of zero, first and second-order kinetic, respectively, and t is the reaction time. The values of rate constants of studied kinetics and their regression coefficients are presented in Table 3.

Based on the R^2_{adj}, the degradation of DR89 was followed by first-order reaction kinetics in LED radiation, Bi_2O_3/TiO_2 adsorption, and Bi_2O_3/TiO_2 photocatalysis processes (Table 3 and Fig. 7).

Many studies have shown that the decomposition of the pollutants in the photocatalytic oxidation process follows the first-order kinetic model [33]. As presented in Table 3, the significant enhancement of the DR89 removal rate ($k_{\text{LED light+Bi}_2\text{O}_3/\text{TiO}_2}$: 0.012 mg/L min) was observed during the application of the Bi_2O_3/TiO_2 photocatalysis process. The synergistic effect between LED light and Bi_2O_3/TiO_2 could be quantified as the normalized difference between the rate constants obtained under Bi_2O_3/TiO_2 photocatalysis and the sum of the separate LED light and Bi_2O_3/TiO_2 rate constants. Eq. (4) was used to evaluate the synergistic effect on the DR89 removal rate in the Bi_2O_3/TiO_2 photocatalysis process.

$$\text{Synergetic effect} = \frac{k_{\text{LED light + Bi}_2\text{O}_3/\text{TiO}_2}}{k_{\text{LED light}} + k_{\text{Bi}_2\text{O}_3/\text{TiO}_2}} = 1.9 \quad (4)$$

The rate constant of the Bi_2O_3/TiO_2 photocatalysis was around twice (0.012–0.0064) the sum of the individual LED light and Bi_2O_3/TiO_2 processes.

3.2.4. Effect of Bi_2O_3/TiO_2 composite dose

By applying different doses of Bi_2O_3/TiO_2 composite in photocatalysis experiments, the effect of catalyst dose on DR89 removal efficiency has been investigated and the obtained results are revealed in Fig. 8.

As illustrated in Fig. 8, the removal efficiency of DR89 by Bi_2O_3/TiO_2 photocatalysis was increased from 60.7% to 94.8% with increasing the dose of Bi_2O_3/TiO_2 composite from 100 to 800 mg/L. This situation was presumably related to the increase in the surface area and the number of active sites on the Bi_2O_3/TiO_2 composite surface. Consequently, the generation of electron–hole pairs on the surface of the catalyst was increased and led to the higher production of $^{\bullet}OH$ radicals and resulted in higher DR89 removal efficiency [24]. Eqs. (5)–(8) show the formation of the reaction of $^{\bullet}OH$ by the photocatalytic process [34].

$$h^+ + H_2O \rightarrow H^+ + {}^{\bullet}OH \quad (5)$$

$$h^+ + OH^- \rightarrow {}^{\bullet}OH \quad (6)$$

$$e^- + O_2 \rightarrow {}^{\bullet}O_2^- \quad (7)$$

$${}^{\bullet}O_2^- + H_2O + H^+ \rightarrow H_2O_2 + OH^- \quad (8)$$

$$H_2O_2 + e^- \rightarrow {}^{\bullet}OH + OH^- \quad (9)$$

In addition, another reason for more efficient removal with the increasing catalyst dose was that the number of dye molecules adsorption on catalyst surface was increased [35]. Fu et al. [36] indicated that LR5B degradation efficiency enhanced when the catalyst dose increased from 10 to 80 mg/L. Furthermore, Uheida et al. [24] demonstrated that the dose of catalyst is an effective parameter in the destruction of organic pollutants and degradation efficiency was improved by increasing the catalyst dose. An overview of previously published research on organic pollutant degradation by different photocatalysts is summarized in Table 4.

3.2.5. Effect of initial DR89 concentration

The variations of DR89 removal efficiency by Bi_2O_3/TiO_2 photocatalysis as a function of initial DR89 concentration are depicted in Fig. 9.

As depicted in Fig. 9, the DR89 removal efficiency was raised with increasing initial DR89 concentration from 10 to 20 mg/L and then the steepness trend of removal efficiency was observed with increasing initial

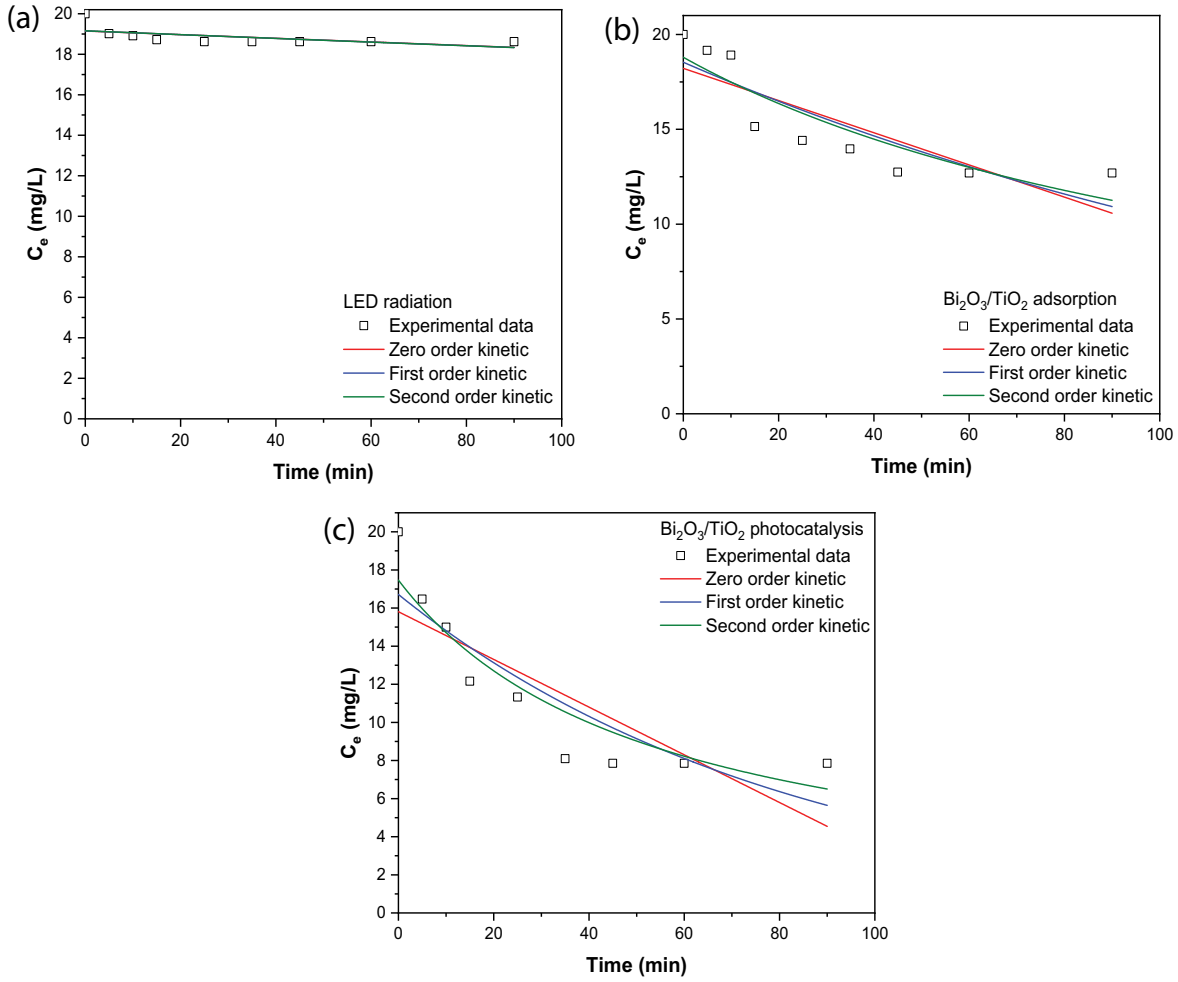

Fig. 7. The non-linear fitted plot of kinetic models of DR89 removal by (a) LED radiation, (b) Bi_2O_3/TiO_2 adsorption, and (c) Bi_2O_3/TiO_2 photocatalysis.

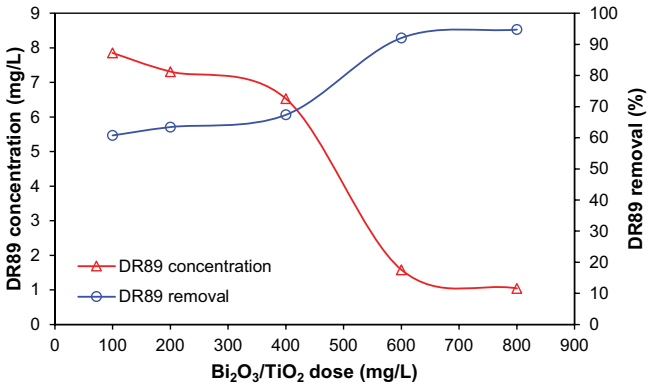

Fig. 8. Effect of different Bi_2O_3/TiO_2 composite dose on DR89 removal efficiency (DR89 concentration: 20 mg/L; solution pH: 4; reaction time: 45; LED as a light source).

DR89 concentration. The results of this study are in line with the findings reported by Rahimi et al. [40]. Further, some studies reported that dye degradation efficiency was reduced with an increase in dye concentration [46,47]. The decreasing trend of dye degradation with high initial concentrations is due to (i) the constant number of active catalyst positions [48], (ii) the production of •OH is constant at all dye concentrations and the reaction between dye molecules and •OH radical decreases [49], and (iii) the dye molecules acts as a filter and reduces the penetration of radiated beam [50]. The radical formation during the photocatalysis process with Bi_2O_3/TiO_2 composite under LED and UV-C irradiation are illustrated in Fig. 10.

3.2.6. Irradiation source type

Fig. 11 illustrates a comparison of DR89 removal efficiency with Bi_2O_3/TiO_2 photocatalysis by using UV-C and LED irradiation as a light source.

As can be seen, the DR89 removal efficiency by Bi_2O_3/TiO_2 photocatalysis under LED radiation at a low initial concentration of DR89 (10 mg/L) was significantly higher than Bi_2O_3/TiO_2 photocatalysis by UV-C radiation. Siddiqa et al. [51] studied the removal of dyes and phenol and indicated that the photocatalytic performance of the nanocomposites under visible light irradiations was much higher than for UV irradiation. Furthermore, higher initial DR89

Table 4
Removal of organic pollutants using different photocatalysts

Catalyst type	Catalyst does (mg/L)	Contaminate	Concentration (mg/L)	pH	Reaction time (min)	Light source	Degradation (%)	References
Bi_2O_3/TiO_2	500	Ofloxacin	25	7	120	Solar	92.4	[19]
Bi_2O_3/TiO_2	1,000	Dibutyl phthalate	5	–	240	Visible	45	[8]
Bi_2O_3/TiO_2	–	Orange II	50	–	220	UV-Vis	100	[37]
Bi_2O_3/TiO_2	50	Quinalphos	25	8	100	Visible	92	[25]
$Ag/Bi_2O_3/TiO_2$	–	Methyl orange		–	180	UV	99	[38]
$Cu\text{-}Bi_2O_3\text{-}TiO_2$	1,200	Methyl orange	10	4	–	Visible	74	[33]
GO/TiO_2	1,000	Rhodamine B	20	4	120	UV-Vis	100	[39]
$BiVO_4/TiO_2$-zeolite	1,700	Acid orange 10	10	3	50	Visible	99.9	[40]
$Fe_3O_4@SiO_2@TiO_2/rGO$	200	2,4-dinitrophenol	40	7	30	UV	88.8	[41]
$BiVO_4/TiO_2$	2,000	Arsenic	3	4.5	120	LED	99.9	[42]
TiO_2/Fe_3O_4/multi-walled carbon nanotubes	100	1-methylimidazole-2-thiol	10		60	UV	82.7	[43]
TiO_2	50	Ibuprofen	–	7	60	UV	80	[44]
TiO_2/AB/PS	500	Tetracycline	30	–	120	Visible	93.3	[45]
Bi_2O_3/TiO_2	800	DR89	20	4	45	LED	94.8	Present study

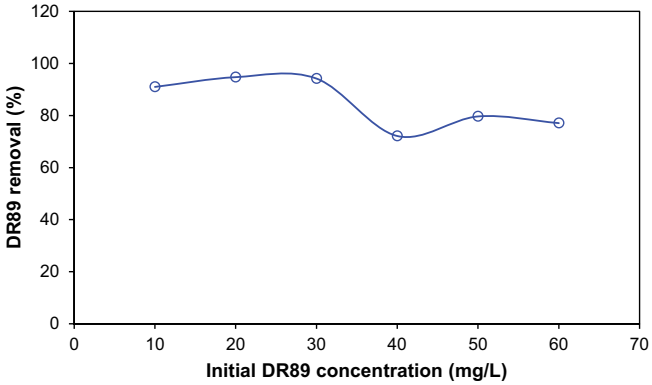

Fig. 9. DR89 removal efficiency by Bi_2O_3/TiO_2 photocatalysis as a function of initial DR89 concentration (solution pH: 4; reaction time: 45 min; Bi_2O_3/TiO_2 dose: 800 mg/L; LED as a light source).

concentration led to approximately equal DR89 removal efficiency under LED and UV-C radiation. The LED lamps were suggested as a light source in this study due to many drawbacks related to the UV lamps including fragility, the danger of explosion for their high pressures, working temperatures, and the hazardous and toxic substances in UV lamp structure, and the advantages of LED lamps [12].

3.2.7. Effect of co-existing cations and anions

In order to study the effect of co-existing cations and anions on the photocatalytic activity of Bi_2O_3/TiO_2 composite, the mono, di, and trivalent co-existing cations and anions including Na^+, K^+, Mg^{2+}, Ca^{2+}, Cl^-, SO_4^{2-} and PO_4^{3-} were selected. The Bi_2O_3/TiO_2 photocatalysis experiments were carried out at the constant concentration of co-existing cations and anions (5 mmol/L) using LED and UV-C as a light source (Fig. 12).

As observed in Fig. 12, the presence of co-existing anions in both photocatalytic systems have a more pronounced effect comparing with co-existing cations, and the highest inhibiting effects on DR89 removal efficiency are related to PO_4^{3-} ions. The effect of co-existing anions on the photocatalytic activity of Bi_2O_3/TiO_2 composite is summarized in the reducing order as shown below.

$$PO_4^{3-} > Cl^- > SO_4^{2-}$$

The previous study reported that the presence of anions would change the ionic strength of the medium as well as the generation of various radical species, influencing the degradation efficiency of organic pollutants [52]. The sulfate ions react with holes and $^{\bullet}OH$ radicals and produce sulfate radicals ($SO_4^{-\bullet}$) based on Eqs. (10) and (11).

$$SO_4^{2-} + {}^{\bullet}OH \rightarrow SO_4^{-\bullet} + OH^- \quad (10)$$

$$SO_4^{2-} + h^+ \rightarrow SO_4^{-\bullet} \quad (11)$$

Hence, the amount of holes and $^{\bullet}OH$ radicals reduced [53] and $^{\bullet}OH$ radicals are more reactive than $SO_4^{-\bullet}$ radical [41]. In case of Cl^- ions, it can scavenge the holes in the photocatalysis system and reduce the yield of the *in-situ* H_2O_2 formation based on the Eqs. (12) and (13) [54].

$$Cl^- + {}^{\bullet}OH \rightarrow Cl^{\bullet} + OH^- \quad (12)$$

$$Cl^+ + h^+ \rightarrow Cl^{\bullet} \quad (13)$$

Eskandarloo et al. [52] studied triphenylmethane dye removal and indicated that the dye degradation efficiency

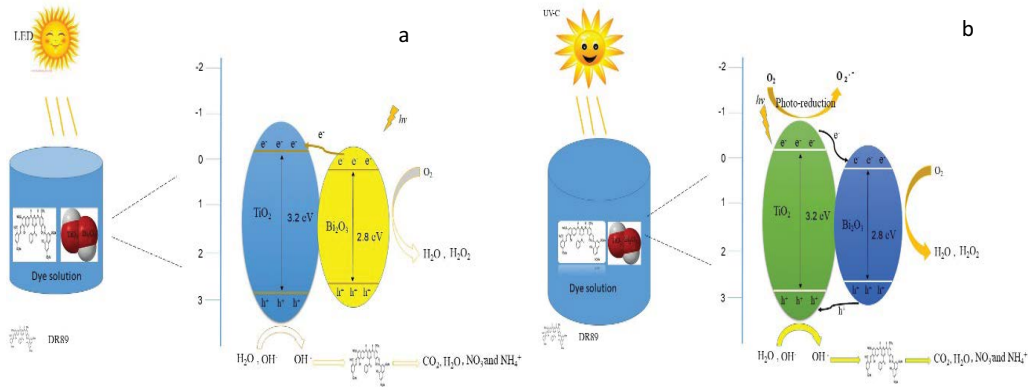

Fig. 10. Mechanism of photocatalytic reaction on the Bi_2O_3/TiO_2 catalyst: (a) LED irradiation and (b) UV-C radiation.

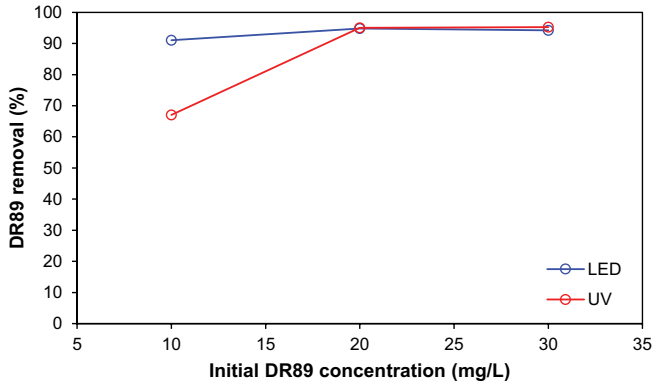

Fig. 11. Variation of DR89 removal by Bi_2O_3/TiO_2 photocatalysis under LED and UV-C radiation (solution pH: 4; reaction time: 45 min; Bi_2O_3/TiO_2 dose: 800 mg/L).

decreased with SO_4^{2-} and Cl^- addition into the medium. The degradation efficiency of DR89 is significantly inhibited in the presence of PO_4^{3-}. This result may be attributed to the increased charge of PO_4^{3-} ions. The photo-generated holes can be consumed by PO_4^{3-}, which can be converted to $H_2PO_4^-$ and $H_2PO_4^{2-}$ ions. The HPO_4^{2-} ions can capture photo-generated holes and can be converted to $H_2PO_4^-$ ions [55]. In addition, the presence of $H_2PO_4^-$ in solution leads to lowers the photocatalysis efficiency by scavenging $^{\bullet}OH$ radicals as shown in Eq. (14) [56].

$$HO^{\bullet} + H_2PO_4^- \rightarrow OH^- + H_2PO_4^{\bullet} \quad (14)$$

Fu et al. [36] investigated the influence of the PO_4^{3-} ions as co-existing anion on the decomposition of Lanasol Red 5B and concluded that the presence of PO_4^{3-} ions inhibit the degradation efficiency of the photocatalysis process.

As illustrated in Fig. 12, the presence of K^+ ions as co-existing cations showed promoting effects on DR89 removal efficiency by Bi_2O_3/TiO_2 photocatalysis under LED irradiation. This result may be attributed to the adsorption of K^+ cation at the interface of Bi_2O_3/TiO_2 composite and electrolyte and lead to the more positive surface charge of catalyst. Therefore, the interactions between the dye molecules and the catalyst surface increased, and consequently, the degradation efficiency of the photocatalysis process increased [57].

In addition, the presence of Na^+ cation in the photocatalytic system was depicted to have a more inhibiting effect on DR89 removal efficiency than other studied cations. The overall DR89 removal efficiency drops by Bi_2O_3/TiO_2

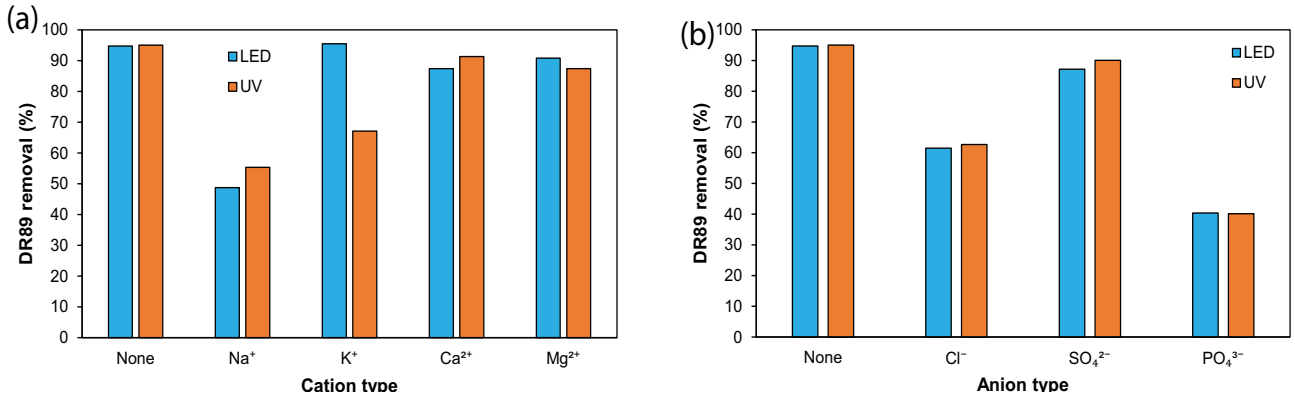

Fig. 12. Effect of co-existing (a) cations and (b) anions on photocatalytic activity of Bi_2O_3/TiO_2 composite (DR89 concentration: 20 mg/L; solution pH: 4; reaction time: 45; Bi_2O_3/TiO_2 dose: 800 mg/L; LED and UV-C as light source).

photocatalysis using LED as a light source are summarized as follows.

$$Na^+ > Ca^{2+} > Mg^{2+}$$

Similar results have been presented by Fu et al [36], demonstrating that the degradation efficiency of Lanasol Red 5B decreased from 95% to 87% with the application of Ca^{2+} ions as co-existing cations. By adding Ca^{2+} and Mg^{2+} ions, the photocatalytic decomposition of DR89 was decreased, which may be due to the reaction of Ca^{2+} and Mg^{2+} with DR89 molecules or intermediates to form stable metal complexes, which are more difficult to be degraded [36,58]. Fan et al. [59] stated the presence of Mg^{2+} ions in the medium slightly inhibited the photocatalytic degradation of naproxen.

In case of UV-C irradiation, the reduction of DR89 removal efficiency for studied cations was in the order of $Na^+ > K^+ > Mg^{2+} > Ca^{2+}$.

When UV-C was used as a light source in Bi_2O_3/TiO_2 photocatalysis, the divalent cations (Mg^{2+} and Ca^{2+}) showed a lower depleting effect on DR89 removal efficiency comparing with monovalent cations (Na^+ and K^+). This was presumably related to high ionic strength due to the existing cations in medium and preventing the electrostatic repulsive by a compression of the electric double layer due to high valency. The strong electrostatic field of cations was the most efficient at compressing the electric double [43].

3.2.8. Application of persulfate as additives

The performance of Bi_2O_3/TiO_2 photolysis in DR89 removal was investigated by adding the PS under LED and UV-C irradiation. Fig. 13 illustrates the effect of various PS doses (2.5–12.5 mg/L) on the decomposition efficiency of DR89.

As shown in Fig. 12, the highest removal efficiency of DR89 under LED and UV-C irradiation was observed at PS dose of 2.5 and 5 mg/L, respectively. The increase of removal efficiency could be ascribed to the generation of photo-induced electron and hole under UV-C and LED irradiation which reacted with PS to form more $SO_4^{-\bullet}$ radical. Thus, the highly active $^\bullet OH$ radicals are generated with the subsequent reaction of $SO_4^{-\bullet}$ radical and water molecules. As a result, the aromatic rings of DR89 could be effectively broken down with the combination of $^\bullet OH$ and $SO_4^{-\bullet}$ radicals [60]. The main reaction processes are listed below (Eqs. (15)–(18)) [61].

$$S_2O_8^{2-} + 2e^- \rightarrow 2SO_4^{2-} \quad (15)$$

$$S_2O_8^{2-} + h\nu \rightarrow 2SO_4^{-\bullet} \quad (16)$$

$$2SO_4^{-\bullet} + H_2O \rightarrow 2SO_4^{2-} + {}^\bullet OH + H^+ \quad (17)$$

$$SO_4^{2-} + {}^\bullet OH \rightarrow SO_4^{-\bullet} + OH^- \quad (18)$$

Zhang et al. [45] reported that with increasing PS dose from 0 to 3 mmol/L, the tetracycline decomposition increased and the degradation of tetracycline decreased by applying the PS dose higher than 3 mmol/L. This behavior was presumably related to this fact that $SO_4^{-\bullet}$ radicals scavenging would occur at higher PS concentrations based on Eqs. (19) and (20). Furthermore, $SO_4^{-\bullet}$ was more reactive than $S_2O_8^{-\bullet}$ [62].

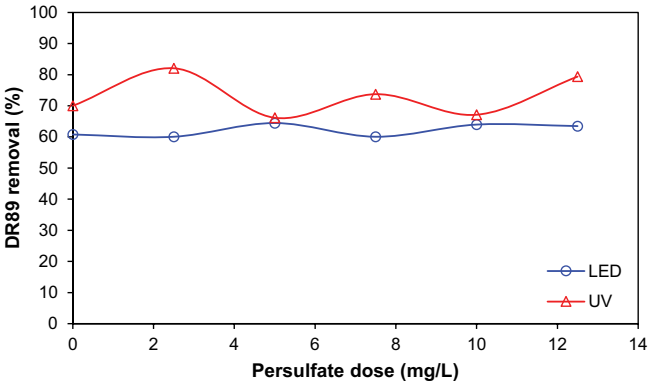

Fig. 13. Variation of DR89 removal efficiency by Bi_2O_3/TiO_2 photocatalysis with persulfate surplus (DR89 concentration: 20 mg/L; solution pH: 4; reaction time: 45; Bi_2O_3/TiO_2 dose: 100 mg/L).

$$SO_4^{-\bullet} + S_2O_8^{2-} \rightarrow S_2O_8^{-\bullet} + SO_4^{2-} \quad (19)$$

$$SO_4^{-\bullet} + SO_4^{-\bullet} \rightarrow S_2O_8^{2-} \quad (20)$$

3.3. ANN modeling

In the present study, the ANN was constructed by determining the number of layers, the number of nodes in each layer, and the nature of the transfer functions to predict the removal by the Bi_2O_3/TiO_2 photocatalysis process. The ANN topology optimization is presumably the critical steps in the model development. In this study, a three-layered, feed-forward back-propagation neural network was used. The ANN examined in the present study was comprised of four inputs parameters including solution pH, reaction time, Bi_2O_3/TiO_2 dose, and initial DR89 concentration. Table 1 summarizes the range of studied parameters. The output layer comprised one neuron representing DR89 removal efficiency. In order to feed the ANN structure, 26 experimental sets were randomly divided into training (70%), validation (15%), and test subsets (15%). Since the used transfer function in the hidden layer was sigmoid; all samples should be scaled into the 0.1–0.9 range according to Eq. (21).

$$x_{i,\text{norm}} = \left(0.8\frac{x_i - x_{i,\min}}{x_{i,\max} - x_{i,\min}}\right) + 0.1 \quad (21)$$

where $x_{i,\min}$ and $x_{i,\max}$ represent the lowest and highest values of variable x_i. The sigmoidal transfer function was used as a transfer function in the hidden and output layers. This is the most widely used transfer function, given by Eq. (22).

$$f(x) = \frac{1}{1+\exp(-x)} \quad (22)$$

where $f(x)$ represents the hidden neuron output. In order to optimize ANN, the different numbers of neurons ranging from 2 to 20 in the hidden layer were examined and judged based on the minimum value of the mean square error (MSE) of the training and validation sets (Fig. 14).

A good method for choosing the number of training epoch is to use the validation data set periodically to compute the error rate for it while the ANN is being trained. Fig. 15 shows the progress of the MSE with the number of iterations of training, validation, and test.

As seen in Fig. 15, the MSE decreases in the early epochs of backpropagation but after a while, it begins to increase. The obtained results indicated that the minimum MSE of the validation set could be achieved in the epochs about 11. After 11 epochs, the MSE slightly increased. Therefore, 11 epochs were selected as the optimum epoch number. The optimized ANN consisted of input, hidden and output layers of 4, 13, and 1, respectively, which was used to the modeling of DR89 removal efficiency by photocatalysis (Fig. 16).

The precision of the ANN model was investigated with a comparison between predicted values and experimental data. It should be noted that each topology was repeated three times to avoid random correlation due to the random initialization of the weights. Fig. 17 shows a comparison between normalized experimental and predicted values of DR89 removal efficiency by using the optimum neural network model with 13 neurons in the hidden layer.

The plot in Fig. 17 has a correlation coefficient of 0.993 for the test set which confirmed that the ANN model is a good method of predicting the experimental data within the adopted ranges. All the DR89 removal efficiency performed an inverse range scaling to return the predicted responses to their original scale and compared them with experimental responses (Fig. 18).

These results confirm that the ANN model reproduces the DR89 removal efficiency in the photocatalysis process within the experimental ranges adopted in the model fitting. The relative importance of input parameters on the DR89 removal efficiency was computed based on the partitioning of connection weights (Eq. (23)).

$$I_j = \frac{\sum_{m=1}^{m=N_h}\left(\left(\left|W_{jm}^{ih}\right| \div \sum_{k=1}^{k=N_i}\left|W_{km}^{ih}\right|\right)\times\left|W_{mn}^{ho}\right|\right)}{\sum_{k=1}^{k=N_i}\left[\sum_{m=1}^{m=N_h}\left(\left(\left|W_{jm}^{ih}\right| \div \sum_{k=1}^{k=N_i}\left|W_{km}^{ih}\right|\right)\times\left|W_{mn}^{ho}\right|\right)\right]} \tag{23}$$

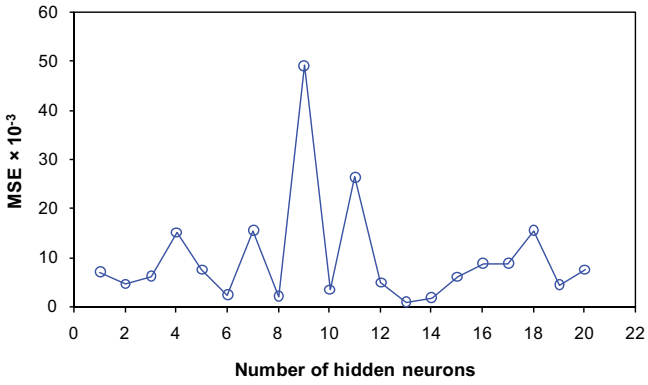

Fig. 14. Performance of ANN as a function of neurons number in the hidden layer.

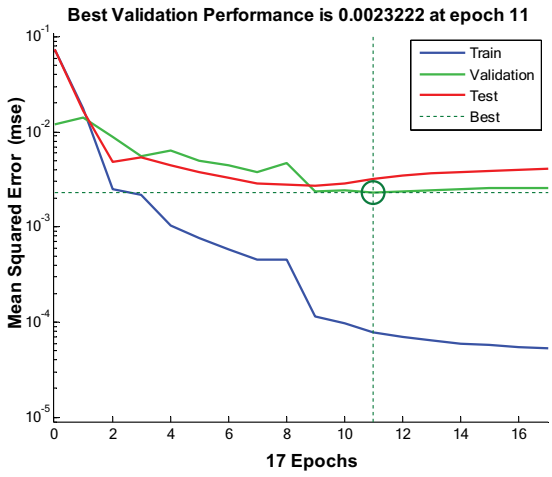

Fig. 15. MSE progress with the number of iterations of training, validation, and test.

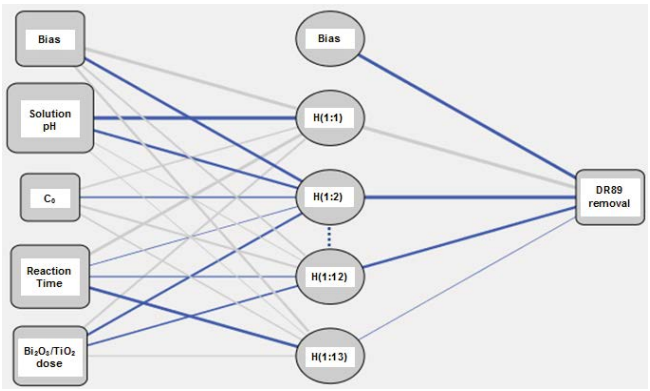

Fig. 16. Structure of optimized ANN.

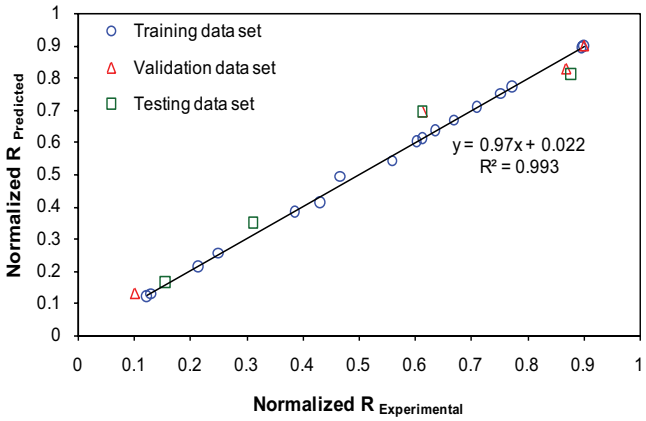

Fig. 17. Comparison of the normalized experimental results of DR89 removal efficiency with ANN predicted for the data set.

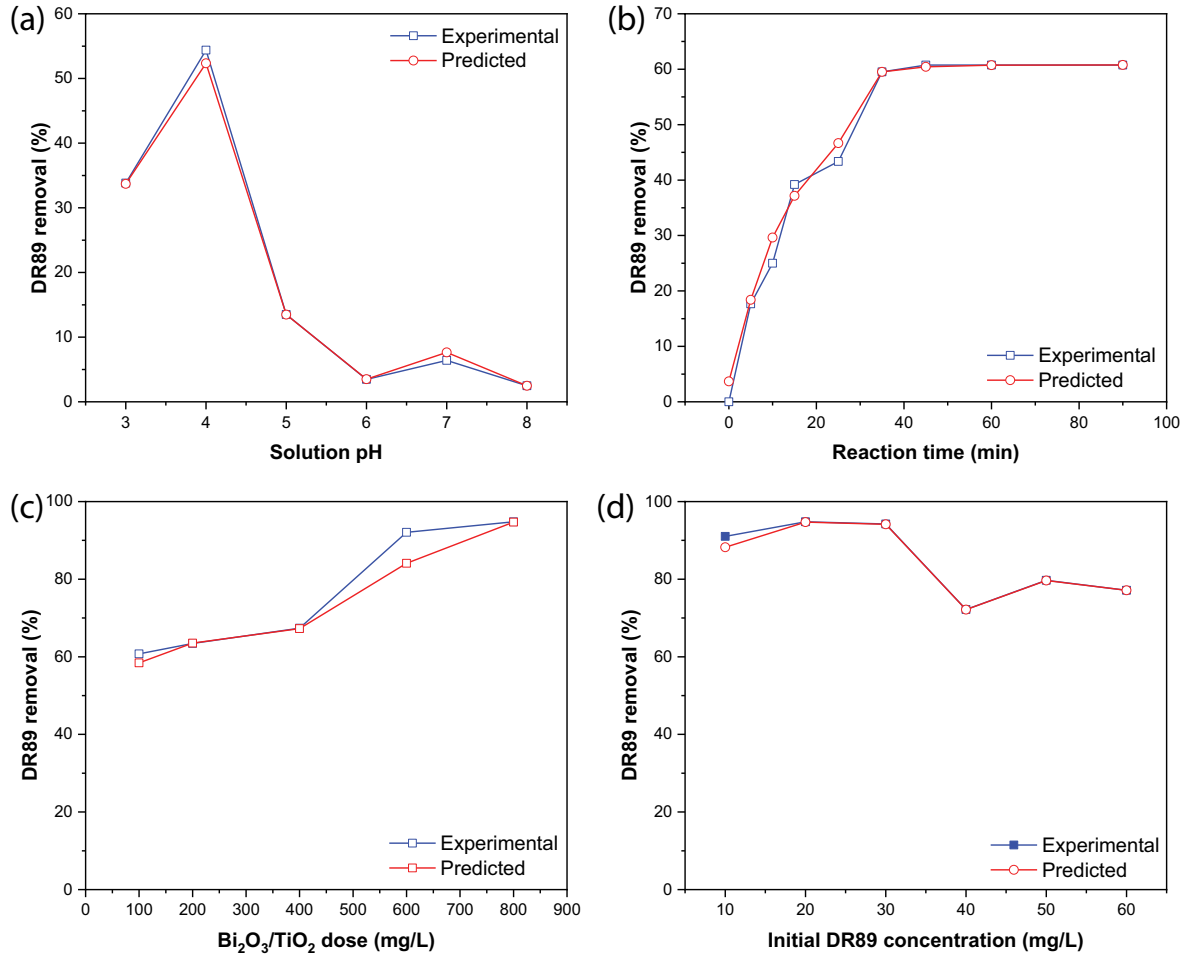

Fig. 18. Comparison between ANN predicted and experimental values of DR89 removal as a function of (a) solution pH, (b) reaction time, (c) Bi_2O_3/TiO_2 dose, and (d) initial DR89 concentration.

where I_j represents the relative importance of the j^{th} input parameters on the output variable, N_i and N_h represent the numbers of input and hidden neurons, respectively; W indicates connection weights, the superscripts "i", "h" and "o" refer to input, hidden and output layers, respectively; and subscripts "k", "m" and "n" refer to input, hidden and output neurons, respectively. The calculated relative importance of various input parameters is shown in Fig. 19.

As seen in Fig. 19, all independent parameters (solution pH, reaction time, Bi_2O_3/TiO_2 dose, and initial DR89 concentration) strongly influence the DR89 removal efficiency and none of the parameters could be neglected in the present analysis. However, the solution pH with a relative importance of 37.5% appeared to be the most influential parameter in the photocatalysis process.

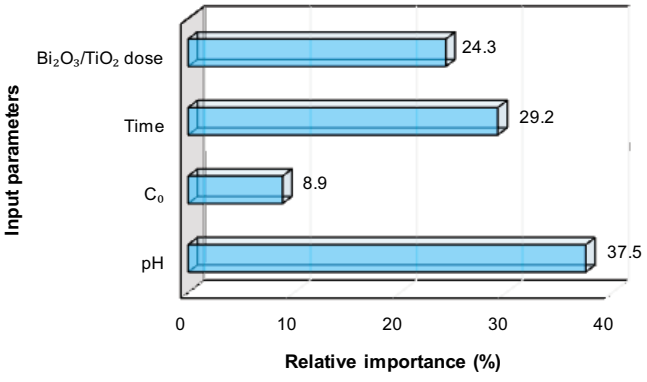

Fig. 19. The relative importance of input parameters on DR89 removal efficiency.

4. Conclusions

In this study, Bi_2O_3/TiO_2 composite has been successfully synthesized by the solvothermal method and BET, EDX, and TEM analysis used for composite characterization. The synthesized Bi_2O_3/TiO_2 composite was subsequently used for DR89 removal efficiency from aqueous solutions under LED and UV-C light irradiation. The kinetic data indicated that the adsorption process was followed by the first-order kinetic model. The results indicated that the optimum conditions for DR89 removal efficiency were solution pH of 4 and a Bi_2O_3/TiO_2 composite dose of 800 at

20 mg/L of initial DR89 concentration. Under optimum conditions, the Bi_2O_3/TiO_2 photocatalysis under LED light was achieved to 94.8% removal efficiency of DR89 at 45 min reaction time. In comparison with other co-existing anions and cations, the PO_4^{3-} ion, showed more inhibition effects on photocatalytic decomposition of DR89. In addition, adding the PS enhanced the DR89 removal efficiency at the concentration of 2.5 and 5 mg/L under UV-C and LED irradiation. The correlation coefficient for ANN was calculated 0.993, confirming that the predicted data from the designed ANN model were in good agreement with the experimental data. The obtained results proposed that the Bi_2O_3/TiO_2 composite under visible light could be efficiently used for photocatalytic degradation of organic pollutants from textile mills and other similar industries.

Acknowledgment

This study was conducted at IUMS in 2019 under Project No. 397717 with ethical code #IR.MUI.RESEARCH.REC.1397.464. We appreciate the financial support from IUMS, Isfahan, Iran.

References

[1] T.R. Waghmode, M.B. Kurade, R.T. Sapkal, C.H. Bhosale, B.-H. Jeon, S.P. Govindwar, Sequential photocatalysis and biological treatment for the enhanced degradation of the persistent azo dye methyl red, J. Hazard. Mater., 371 (2019) 115–122.

[2] B. Boutra, M. Trari, Solar photodegradation of a textile azo dye using synthesized ZnO/bentonite, Water Sci. Technol., 75 (2017) 1211–1220.

[3] P. Mondal, S. Baksi, D. Bose, Study of environmental issues in textile industries and recent wastewater treatment technology, World Sci. News, 61 (2017) 98–109.

[4] C.B. Ong, L.Y. Ng, A.W. Mohammad, A review of ZnO nanoparticles as solar photocatalysts: synthesis, mechanisms and applications, Renewable Sustainable Energy Rev., 81 (2018) 536–551.

[5] A.H. Ali, S. Kapoor, S.K. Kansal, Studies on the photocatalytic decolorization of pararosanilne chloride dye and its simulated dyebath effluent, Desal. Water Treat., 25 (2011) 268–275.

[6] J.G. Wang, P. Zhang, X. Li, J. Zhu, H.X. Li, Synchronical pollutant degradation and H_2 production on a Ti^{3+}-doped TiO_2 visible photocatalyst with dominant (0 0 1) facets, Appl. Catal., B, 134 (2013) 198–204.

[7] H. Liu, X.N. Dong, X.C. Wang, C.C. Sun, J.Q. Li, Z.F. Zhu, A green and direct synthesis of graphene oxide encapsulated TiO_2 core/shell structures with enhanced photoactivity, Chem. Eng. J., 230 (2013) 279–285.

[8] S.Z. You, Y. Hu, X.C. Liu, C.H. Wei, Synergetic removal of Pb(II) and dibutyl phthalate mixed pollutants on Bi_2O_3-TiO_2 composite photocatalyst under visible light, Appl. Catal., B, 232 (2018) 288–298.

[9] B. Neppolian, L. Ciceri, C.L. Bianchi, F. Grieser, M. Ashokkumar, Sonophotocatalytic degradation of 4-chlorophenol using Bi_2O_3/$TiZrO_4$ as a visible light responsive photocatalyst, Ultrason. Sonochem., 18 (2011) 135–139.

[10] V. Vaiano, G. Iervolino, L. Rizzo, Cu-doped ZnO as efficient photocatalyst for the oxidation of arsenite to arsenate under visible light, Appl. Catal., B, 238 (2018) 471–479.

[11] J.H. Feng, Y.Y. Li, Z.Q. Gao, H. Lv, X.B. Zhang, D.W. Fan, Q. Wei, Visible-light driven label-free photoelectrochemical immunosensor based on TiO_2/S-$BiVO_4$@Ag_2S nanocomposites for sensitive detection OTA, Biosens. Bioelectron., 99 (2018) 14–20.

[12] V. Vaiano, O. Sacco, D. Sannino, Electric energy saving in photocatalytic removal of crystal violet dye through the simultaneous use of long-persistent blue phosphors, nitrogen-doped TiO_2 and UV-light emitting diodes, J. Cleaner Prod., 210 (2019) 1015–1021.

[13] L. Das, U. Maity, J.K. Basu, The photocatalytic degradation of carbamazepine and prediction by artificial neural networks, Process Saf. Environ. Prot., 92 (2014) 888–895.

[14] S. Agarwal, I. Tyagi, V.K. Gupta, M. Ghaedi, M. Masoomzade, A.M. Ghaedi, B. Mirtamizdoust, Kinetics and thermodynamics of methyl orange adsorption from aqueous solutions—artificial neural network-particle swarm optimization modeling, J. Mol. Liq., 218 (2016) 354–362.

[15] D. Podstawczyk, A. Witek-Krowiak, A. Dawiec, A. Bhatnagar, Biosorption of copper(II) ions by flax meal: empirical modeling and process optimization by response surface methodology (RSM) and artificial neural network (ANN) simulation, Ecol. Eng., 83 (2015) 364–379.

[16] S. Mandal, S. Mahapatra, R.K. Patel, Enhanced removal of Cr(VI) by cerium oxide polyaniline composite: optimization and modeling approach using response surface methodology and artificial neural networks, J. Environ. Chem. Eng., 3 (2015) 870–885.

[17] L.F. Yin, J.F. Niu, Z.Y. Shen, J. Chen, Mechanism of reductive decomposition of pentachlorophenol by Ti-doped β-Bi_2O_3 under visible light irradiation, Environ. Sci. Technol., 44 (2010) 5581–5586.

[18] C. Karunakaran, P. Magesan, P. Gomathisankar, Photocatalytic activity of sol–gel derived Bi_2O_3-TiO_2 nanocomposite, Mater. Sci. Forum, 712 (2012) 73–83.

[19] S. Sood, S.K. Mehta, A.S.K. Sinha, S.K. Kansal, Bi_2O_3/TiO_2 heterostructures: synthesis, characterization and their application in solar light mediated photocatalyzed degradation of an antibiotic, ofloxacin, Chem. Eng. J., 290 (2016) 45–52.

[20] J.L. Wang, X.D. Yang, K. Zhao, P.F. Xu, L.B. Zong, R.B. Yu, D. Wang, J.X. Deng, J. Chen, X.R. Xing, Precursor-induced fabrication of β-Bi_2O_3 microspheres and their performance as visible-light-driven photocatalysts, J. Mater. Chem. A, 1 (2013) 9069–9074.

[21] A. Habibi-Yangjeh, S. Feizpoor, D. Seifzadeh, S. Ghosh, Improving visible-light-induced photocatalytic ability of TiO_2 through coupling with Bi_3O_4Cl and carbon dot nanoparticles, Sep. Purif. Technol., 238 (2020) 116404, https://doi.org/10.1016/j.seppur.2019.116404.

[22] P.Y. Ayekoe, D. Robert, D.L. Goné, Preparation of effective TiO_2/Bi_2O_3 photocatalysts for water treatment, Environ. Chem. Lett., 14 (2016) 387–393.

[23] O. Bechambi, S. Sayadi, W. Najjar, Photocatalytic degradation of bisphenol A in the presence of C-doped ZnO: effect of operational parameters and photodegradation mechanism, J. Ind. Eng. Chem., 32 (2015) 201–210.

[24] A. Uheida, A. Mohamed, M. Belaqziz, W.S. Nasser, Photocatalytic degradation of Ibuprofen, Naproxen, and Cetirizine using PAN-MWCNT nanofibers crosslinked TiO_2-NH_2 nanoparticles under visible light irradiation, Sep. Purif. Technol., 212 (2019) 110–118.

[25] D. Sud, A. Syal, Investigations on the phase transformation, optical characteristics, and photocatalytic activity of synthesized heterostructured nanoporous Bi_2O_3-TiO_2, J. Chin. Chem. Soc., 63 (2016) 776–783.

[26] V.K. Gupta, R. Jain, A. Mittal, T.A. Saleh, A. Nayak, S. Agarwal, S. Sikarwar, Photo-catalytic degradation of toxic dye amaranth on TiO_2/UV in aqueous suspensions, Mater. Sci. Eng., C, 32 (2012) 12–17.

[27] R. Abazari, A.R. Mahjoub, G. Salehi, Preparation of amine functionalized g-C_3N_4@$^{H/S}$MOF NCs with visible light photocatalytic characteristic for 4-nitrophenol degradation from aqueous solution, J. Hazard. Mater., 365 (2019) 921–931.

[28] Z.J. Cheng, L. Zhang, X. Guo, X.H. Jiang, T. Li, Adsorption behavior of direct red 80 and congo red onto activated carbon/surfactant: process optimization, kinetics and equilibrium, Spectrochim. Acta, Part A, 137 (2015) 1126–1143.

[29] A.K.L. Sajjad, S. Shamaila, B. Tian, F. Chen, J.L. Zhang, Comparative studies of operational parameters of degradation of azo dyes in visible light by highly efficient WO_x/TiO_2 photocatalyst, J. Hazard. Mater., 177 (2010) 781–791.
[30] P. Nuengmatcha, P. Porrawatkul, S. Chanthai, P. Sricharoen, N. Limchoowong, Enhanced photocatalytic degradation of methylene blue using Fe_2O_3/graphene/CuO nanocomposites under visible light, J. Environ. Chem. Eng., 7 (2019) 103438, https://doi.org/10.1016/j.jece.2019.103438.
[31] S. Fakhravar, M. Farhadian, S. Tangestaninejad, Excellent performance of a novel dual Z-scheme $Cu_2S/Ag_2S/BiVO_4$ heterostructure in metronidazole degradation in batch and continuous systems: Immobilization of catalytic particles on α-Al_2O_3 fiber, Appl. Surf. Sci., 505 (2020) 144599, https://doi.org/10.1016/j.apsusc.2019.144599.
[32] L. Pirinejad, A. Maleki, B. Shahmoradi, H. Daraei, J.-K. Yang, S.-M. Lee, Synthesis and application of Fe-N-Cr-TiO_2 nanocatalyst for photocatalytic degradation of Acid Black 1 under LED light irradiation, J. Mol. Liq., 279 (2019) 232–240.
[33] V. Barahimi, H. Moghimi, R.A. Taheri, Cu doped TiO_2-Bi_2O_3 nanocomposite for degradation of azo dye in aqueous solution: process modeling and optimization using central composite design, J. Environ. Chem. Eng., 7 (2019) 103078, https://doi.org/10.1016/j.jece.2019.103078.
[34] M.H. Sayadi, S. Sobhani, H. Shekari, Photocatalytic degradation of azithromycin using GO@Fe_3O_4/ZnO/SnO_2 nanocomposites, J. Cleaner Prod., 232 (2019) 127–136.
[35] A. Kumar, B. Subash, B. Krishnakumar, A.J.F.N. Sobral, K.R. Sankaran, Synthesis, characterization and excellent catalytic activity of modified ZnO photocatalyst for RR 120 dye degradation under UV-A and solar light illumination, J. Water Process Eng., 13 (2016) 6–15.
[36] S. Fu, W. Yuan, Y.H. Yan, H.P. Liu, X.K. Shi, F.Y. Zhao, J. Zhou, Highly efficient visible-light photoactivity of Z-scheme MoS_2/Ag_2CO_3 photocatalysts for organic pollutants degradation and bacterial inactivation, J. Environ. Manage., 252 (2019) 109654, https://doi.org/10.1016/j.jenvman.2019.109654.
[37] P.Y. Ayekoe, D. Robert, D.L. Goné, Facile synthesis of TiO_2/Bi_2O_3 heterojunctions for the photocatalytic degradation of water contaminants, Res. Rev. J. Chem., 6 (2017) 77–83.
[38] M. Malligavathy, S. Iyyapushpam, S.T. Nishanthi, D.P. Padiyan, Photoreduction synthesis of silver on Bi_2O_3/TiO_2 nanocomposites and their catalytic activity for the degradation of methyl orange, J. Mater. Sci. - Mater. Electron., 28 (2017) 18307–18321.
[39] M.S. Adly, Sh.M. El-Dafrawy, S.A. El-Hakam, Application of nanostructured graphene oxide/titanium dioxide composites for photocatalytic degradation of rhodamine B and acid green 25 dyes, J. Mater. Res. Technol., 8 (2019) 5610–5622.
[40] B. Rahimi, N. Jafari, A. Abdolahnejad, H. Farrokhzadeh, A. Ebrahimi, Application of efficient photocatalytic process using a novel BiVO/TiO_2-NaY zeolite composite for removal of acid orange 10 dye in aqueous solutions: Modeling by response surface methodology (RSM), J. Environ. Chem. Eng., 7 (2019) 103253, https://doi.org/10.1016/j.jece.2019.103253.
[41] B. Mirza Hedayat, M. Noorisepehr, E. Dehghanifard, A. Esrafili, R. Norozi, Evaluation of photocatalytic degradation of 2,4-Dinitrophenol from synthetic wastewater using Fe_3O_4@SiO_2@TiO_2/rGO magnetic nanoparticles, J. Mol. Liq., 264 (2018) 571–578.
[42] B. Rahimi, A. Ebrahimi, Photocatalytic process for total arsenic removal using an innovative $BiVO_4$/TiO_2/LED system from aqueous solution: optimization by response surface methodology (RSM), J. Taiwan Inst. Chem. Eng., 101 (2019) 64–79.
[43] Y.H. Jiang, Y.Y. Luo, Z.Y. Lu, P.W. Huo, W.N. Xing, M. He, J.Q. Li, Y.S. Yan, Influence of inorganic ions and pH on the photodegradation of 1-methylimidazole-2-thiol with TiO_2 photocatalyst based on magnetic multi-walled carbon nanotubes, Bull. Korean Chem. Soc., 35 (2014) 76–82.
[44] E. Kudlek, M. Dudziak, J. Bohdziewicz, Influence of inorganic ions and organic substances on the degradation of pharmaceutical compound in water matrix, Water, 8 (2016) 532, https://doi.org/10.3390/w8110532.
[45] T.H. Zhang, Y.J. Liu, Y.D. Rao, X.P. Li, D.L. Yuan, S.F. Tang, Q.X. Zhao, Enhanced photocatalytic activity of TiO_2 with acetylene black and persulfate for degradation of tetracycline hydrochloride under visible light, Chem. Eng. J., 384 (2020) 123350, https://doi.org/10.1016/j.cej.2019.123350.
[46] B. Rahimi, A. Ebrahimi, N. Mansouri, N. Hosseini, Photodegradation process for the removal of acid orange 10 using titanium dioxide and bismuth vanadate from aqueous solution, Global J. Environ. Sci. Manage., 5 (2019) 43–60.
[47] G. Sreelatha, V. Ageetha, J. Parmar, P. Padmaja, Equilibrium and kinetic studies on reactive dye adsorption using palm shell powder (an agrowaste) and chitosan, J. Chem. Eng. Data, 56 (2010) 35–42.
[48] Y.Q. Tan, M. Chen, Y.M. Hao, High efficient removal of Pb(II) by amino-functionalized Fe_3O_4 magnetic nano-particles, Chem. Eng. J., 191 (2012) 104–111.
[49] B. Krishnakumar, K. Selvam, R. Velmurugan, M. Swaminathan, Influence of operational parameters on photodegradation of Acid Black 1 with ZnO, Desal. Water Treat., 24 (2010) 132–139.
[50] C.Y. Wang, Q.J. Zhu, C.T. Gu, X.P. Luo, C.L. Yu, M. Wu, Photocatalytic degradation of two different types of dyes by synthesized La/Bi_2WO_6, RSC Adv., 6 (2016) 85852–85859.
[51] A. Siddiqa, D. Masih, D. Anjum, M. Siddiq, Cobalt and sulfur co-doped nano-size TiO_2 for photodegradation of various dyes and phenol, J. Environ. Sci., 37 (2015) 100–109.
[52] H. Eskandarloo, A. Badiei, M.A. Behnajady, Study of the effect of additives on the photocatalytic degradation of a triphenylmethane dye in the presence of immobilized TiO_2/NiO nanoparticles: artificial neural network modeling, Ind. Eng. Chem. Res., 53 (2014) 6881–6895.
[53] C. Hu, J.C. Yu, Z. Hao, P.K. Wong, Effects of acidity and inorganic ions on the photocatalytic degradation of different azo dyes, Appl. Catal., B, 46 (2003) 35–47.
[54] A. Asghar, A.A.A. Raman, W.M.A.W. Daud, Advanced oxidation processes for *in-situ* production of hydrogen peroxide/hydroxyl radical for textile wastewater treatment: a review, J. Cleaner Prod., 87 (2015) 826–838.
[55] C. Lai, M.M. Zhang, B.S. Li, D.L. Huang, G.M. Zeng, L. Qin, X.G. Liu, H. Yi, M. Cheng, L. Li, Z. Chen, L. Chen, Fabrication of CuS/$BiVO_4$ (0 4 0) binary heterojunction photocatalysts with enhanced photocatalytic activity for Ciprofloxacin degradation and mechanism insight, Chem. Eng. J., 358 (2019) 891–902.
[56] S. Karthikeyan, A. Titus, A. Gnanamani, A.B. Mandal, G. Sekaran, Treatment of textile wastewater by homogeneous and heterogeneous Fenton oxidation processes, Desalination, 281 (2011) 438–445.
[57] P. Borthakur, P.K. Boruah, N. Hussain, Y. Silla, M.R. Das, Specific ion effect on the surface properties of Ag/reduced graphene oxide nanocomposite and its influence on photocatalytic efficiency towards azo dye degradation, Appl. Surf. Sci., 423 (2017) 752–761.
[58] X.J. Yan, R.L. Bao, S.L. Yu, Effect of inorganic ions on the photocatalytic degradation of humic acid, Russ. J. Phys. Chem. A, 86 (2012) 1318–1325.
[59] G.D. Fan, R.S. Ning, J. Luo, J. Zhang, P. Hua, Y. Guo, Z.S. Li, Visible-light-driven photocatalytic degradation of naproxen by Bi-modified titanate nanobulks: Synthesis, degradation pathway and mechanism, J. Photochem. Photobiol., A, 386 (2020) 112108, https://doi.org/10.1016/j.jphotochem.2019.112108.
[60] T.S. Rad, A. Khataee, S.R. Pouran, Synergistic enhancement in photocatalytic performance of Ce(IV) and Cr(III) co-substituted magnetite nanoparticles loaded on reduced graphene oxide sheets, J. Colloid Interface Sci., 528 (2018) 248–262.
[61] V. Matthaiou, Z. Frontistis, A. Petala, M. Solakidou, Y. Deligiannakis, G.N. Angelopoulos, D. Mantzavinos, Utilization of raw red mud as a source of iron activating the persulfate oxidation of paraben, Process Saf. Environ. Prot., 119 (2018) 311–319.
[62] Y.W. Gao, S.M. Li, Y.X. Li, L.Y. Yao, H. Zhang, Accelerated photocatalytic degradation of organic pollutant over metal-organic framework MIL-53 (Fe) under visible LED light mediated by persulfate, Appl. Catal., B, 202 (2017) 165–174.